

# Mobile Robot Connectivity Maintenance Based on RF Mapping

Mustafa Ayad, Jun Jason Zhang, *Member, IEEE*, Richard Voyles, *Senior Member, IEEE*,  
and Mohammad H. Mahoor, *Senior Member, IEEE*,

**Abstract**—This paper presents a method for proactive robot communication connectivity maintenance based on electromagnetic field (EMF) recognition and signal strength (SS) gradient estimation for mobile robots. To achieve these goals in an efficient manner, we combine EMF recognition method and gradient descent of SS measurements into a proactive robot motion control algorithm in a way that maintains connectivity among mobile robots in the presence of a radio frequency (RF) obstacle. The EMF recognition method utilizes hidden Markov models (HMMs) for learning EMF environments based on SS measurements. The proposed motion control algorithm uses the EMF recognition and gradient method results to drive the robots towards favorable locations in which robots can communicate. The numerical simulation demonstrates promising EMF recognition, robot motion control results and confirms their abilities in proactive robot motion control for connectivity maintenance.

## I. INTRODUCTION

In recent years, the communication network has evolved so that properties like node connectivity and signal strength measurements can be used to maintain the quality of connectivity of the network [1]. The connectivity maintenance of robot networks is essential for effective and efficient robot team operations [2]. A competent connectivity maintenance mechanism is required to achieve robust mobile *ad hoc* networks (MANET) especially if the network is subject to intermittent connections due to adverse environments [3]. Multi-robot exploration for urban search and rescue (USAR) is an example of such an application scenario, where a team of robots is instructed to fan out into an unknown environment to accomplish assigned tasks and then return to the operator [4]. As one way to achieve the goal of proactive network connectivity maintenance, robot motion control using EMF environment recognition and multi-dimensional gradient descent methods is expected to provide a good solution to maintain robot connectivity and repair broken links. In this paper, we focus on two steps in the process: Firstly, the EMF environment recognition based on signal strength measurements is used to learn and recognize adverse environments containing RF obstacles. This approach helps to investigate the relationship between known obstacle types and their impact on EMF strength in different scenarios. Secondly, we estimate the multi-dimensional gradient of mobile robots in the experiment field. However, most existing methods estimate the two-dimensional (2-D) gradient with respect to a fixed signal source and do not extend directly

to estimate the gradient where nodes are mobile. While the estimation in the former case is analogous to regression in a 2-D space, the later requires estimations for a four-dimensional (4-D) space. In [5], the authors' incorporate radio SS information into the exploration algorithm by locally sampling the SS and estimating the 2-D gradient. They determine the 2-D gradient of a mobile robot for a fixed signal source. In [6], the authors' considered a scenario exploiting the 2-D gradient within a cooperating sensor network, to localize and navigate to a fixed radio source. The robot measures SS and estimates the direction of the 2-D gradient along which the robot moves in the next step. In [7], [8], the authors focus on developing tools that allow for online evaluation and mapping of received radio SS. In [9], the authors' approach entails the automated construction of a radio map for a partially known urban environment which can then be used to establish a team of robots and the corresponding control algorithm that drive the team to achieve designated targets while maintaining satisfying link quality. In our simulation, we use known obstacles to study their effects on the RF signal measurements when two robots move around the obstacle. We use wall, cylinder and cage obstacles of different sizes, which are made of perfect electric conductor. Numerical simulations have been conducted to evaluate the feasibility and performance of the proposed EMF environment recognition and gradient based motion control. The proposed methods have presented promising solutions to joint message routing and link maintenance in mobile robot network.

## II. FORMULATION FOR EMF RECOGNITION

EMF environment recognition is based on RF signal strength measurements along the robot trajectory. The method aims to identify and classify the EMF environment shadow type along the robots paths. The HMM result based EMF recognition informs moving robots whether they are under the effects of an obstacle shadow or not. Afterwards, the motion control algorithm based on the HMM results decides the controlled motion to recover from the obstacle shadow and maintain the robots connectivity.

### A. EMF Environment Modeling

In our EMF recognition application scenario, we use two sensors to transmit and receive RF signals at 2.4 GHz, respectively. The sensor measurement is the RF signal strength at the current location of the receiver, which is affected by fading and interference [10]. The robots are positioned in 2-D Cartesian coordinates  $(x_k, y_k)$  at time  $k$ . The 2-D space for

M. Ayad, J. Zhang and M. Mahoor are with the Department of Electrical and Computer Engineering, University of Denver, Denver, CO , 80210 USA. R. Voyles is with the College of Technology, Purdue University, West Lafayette, IN USA.

the EMF is divided into grids. The grid width is  $\Delta_x = L_x/M$  in  $x$ -direction and  $\Delta_y = L_y/N$  in  $y$ -direction. Here,  $L_x$  and  $L_y$  are the length and width of the space, and  $M$  and  $N$  are the number of segments in  $x$ -direction and  $y$ -direction as in Fig. 1 (b).

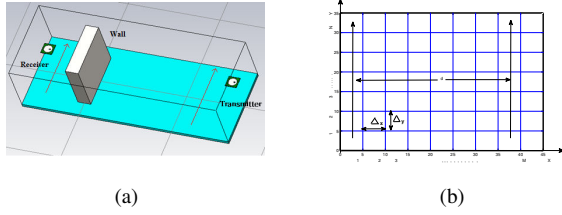


Fig. 1. (a) Experimental scenario with two robots moving on different sides of a wall, and (b) the 2-D space divided into grids in numerical simulation experiments.

In our numerical simulation experiments, we assume that the robots move in this 2-D space along the following trajectories to collect SS measurements. The  $l$ th trajectory is given by

$$x_{k,l}^{(i)} = x_{0,l}^{(i)}, y_{k,l}^{(i)} = y_{0,l}^{(i)} + k\Delta_y, k = 1, 2, \dots, N, \quad (1)$$

where  $l$  is the trajectory index,  $i \in \{1, 2\}$  is the robot index,  $(x_{0,l}^{(i)}, y_{0,l}^{(i)})$  denotes the initial location of the  $i$ th robot at time 0. (1) describes the  $i$ th robot's motion which begins with  $(x_{0,l}^{(i)}, y_{0,l}^{(i)})$  and then moves along  $y$ -direction with a step size of  $\Delta_y$  for each time step. Furthermore, for the 1st robot, we assume  $x_{0,l}^{(1)} = l\Delta_x$ ,  $y_{0,l}^{(1)} = 0$  for the  $l$ th trajectory. For the 2nd robot, we assume  $x_{0,l}^{(2)} = x_{0,l}^{(1)} + d$  and  $y_{0,l}^{(2)} = y_{0,l}^{(1)}$ . The two robots are separated by a fixed distance  $d$  in  $x$ -direction, but they are with the same coordinate in  $y$ -direction. The experiment scenario with two robots is demonstrated in Fig. 1 (a). The sensor measurements at time  $k$  for the  $l$ th trajectory in the presence of obstacle type  $j$ , which is the RF received SS at the receiver location, is denoted as

$$S_l^{(j)}(k) = f(x_{0,l}^{(1)}, y_{0,l}^{(1)}, x_{k,l}^{(1)}, y_{k,l}^{(1)}, x_{0,l}^{(2)}, y_{0,l}^{(2)}, x_{k,l}^{(2)}, y_{k,l}^{(2)}, \phi_j), \quad (2)$$

which is a function of the initial robot positions  $(x_{0,l}^{(i)}, y_{0,l}^{(i)})$ , robots positions  $(x_k^{(i)}, y_k^{(i)})$  at time  $k$  and the obstacle characteristics  $\phi_j$ . Here, the index of the trajectory  $l = 1, \dots, L^{(j)}$  for each  $j$ , where  $L^{(j)}$  is the number of the trajectories with the presence of type  $j$  obstacle. In (2),  $j \in \{1, 2, 3\}$  denotes the obstacle type and  $\phi_j = \{(x_c^{(j)}, y_c^{(j)}), \theta^{(j)}\}$  denotes the obstacle characteristic set. The obstacle characteristic set contains the central position of the obstacle  $(x_c^{(j)}, y_c^{(j)})$  and the shape parameters of the obstacle  $\theta^{(j)}$ . For example, the wall obstacle is with the parameters of central coordination  $(\frac{L_x}{2}, \frac{L_y}{2})$ , and the shape parameters  $\theta^{(j)}$  contains its width, length and height information.

The SS measurements in the experiment field with the presence of three obstacle types are demonstrated in Fig. 2 (a), Fig. 3 (a) and Fig. 4 (a). Fig. 2 (b), Fig. 3 (b) and Fig. 4 (b) show the measurement sequence shapes obtained

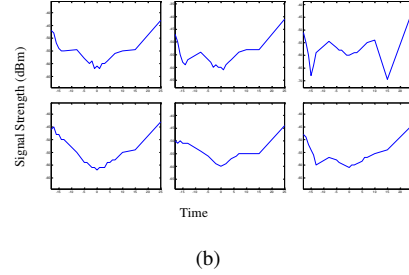
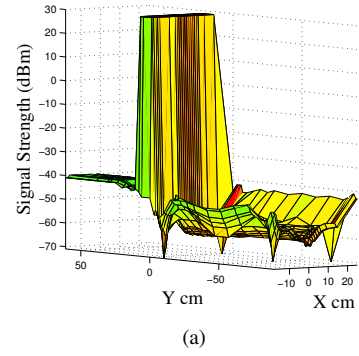


Fig. 2. The RF SS measurements in the 2-D experimental space with the presence of (a) a wall obstacle and (b) RF SS measurement sequences corresponding to different trajectories.

from different trajectories. By investigating how the SS changes at different locations, it is possible to recognize and classify the EMF signatures of certain obstacle types. We used Computer Simulation Technology (CST) Microwave Studio [11] software for EMF simulation and studied three types of obstacles, wall, cage and cylinder for different sizes.

### III. HMM BASED EMF RECOGNITION METHOD

The block diagram in Fig. 6 summarizes the major steps of our algorithm for EMF recognition. First, each measurement vector obtained from different trajectories is segmented into small segments as shown in Fig. 5. Each segment is then transformed into the frequency domain using fast Fourier transform (FFT) for extracting features in the frequency domain. We use a subset of all feature vectors for the training set and the remainder used for the testing set. The extracted feature vectors for training are then clustered using  $K$ -means clustering algorithm to generate observation sequences  $C_l^{(j)}$ . The generated observation sequences are used to train three HMMs, one for each obstacle type. Each HMM model consists of 5 states, corresponding to 5 binned segments of robot motion through a trajectory. As described above, each model was trained using a set of observation sequences. The HMM classification models were tested using the testing set of feature vectors. Using the trained HMM results, the EMF recognition is achieved and then utilized for robot motion control aiming at proactive connectivity maintenance.

The robot motion is a sequential event, and we were interested in classification based on its temporal ordering. There exists a strong analogy of EMF classification using SS measurements to word recognition using speech patterns

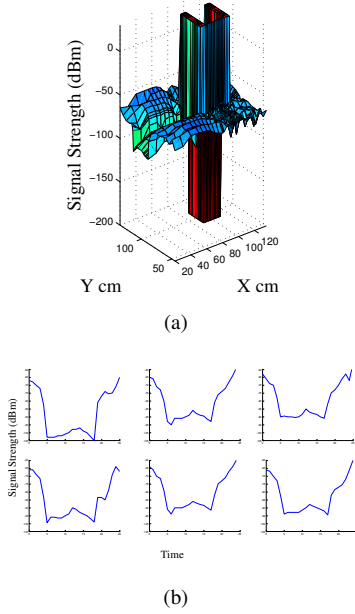


Fig. 3. The RF SS measurements in the 2-D experimental space with the presence of (a) a cage obstacle and (b) Different trajectories.

[12]. The use of HMMs provides an intuitive approach to supervised classification. It naturally breaks up the robot trajectory into constituent parts, similar to the way they are synthesized. The HMM approach also provides a simple mechanism for classifying a subset of segments in the robot trajectory through an obstacle shadow during its movement, as opposed to classification at the completion of a trajectory. The following paragraphs review HMMs and our application of them to EMF recognition.

HMMs [13] is a method to model stochastic events. A model  $\lambda$  consists of states  $Q$  and their corresponding probabilities of observations  $B$ , as well as probabilities of transitions between states  $A$ . Given a sequence of observations,  $O$ , and a model  $\lambda$ , one can drive what is  $P(O|\lambda)$ , the probability of observations  $O$  given  $\lambda$ . Essentially, this is a measure of how well the model represents the event. In the case that the model is unknown (i.e. hidden), the model can be learned. To train a model, training data (a set of observations  $O_i$  for  $(i = 1, \dots, n)$ ) is used to modify an initial estimate of model parameters with the goal of maximizing  $P(O|\lambda)$  using Baum-Welch, EM, or gradient methods. For classification, a model is created for each class  $\lambda_{(j)}$  for  $(j = 1, \dots, m_o)$ , where  $m_o$  is the number of obstacle types. To assign obstacle type membership to a novel observation  $O$ ,  $P(O|\lambda_{(j)})$  is calculated for each type  $j$ , and the class whose model has the highest probability is assigned to  $O$ . The detailed algorithm description and preliminary results are presented as follows.

#### A. Measurement Segmentation and Feature Extraction

We denote the measurement vector collected in the robot movement along the  $l$ th trajectory as  $\beta_l^{(j)} =$

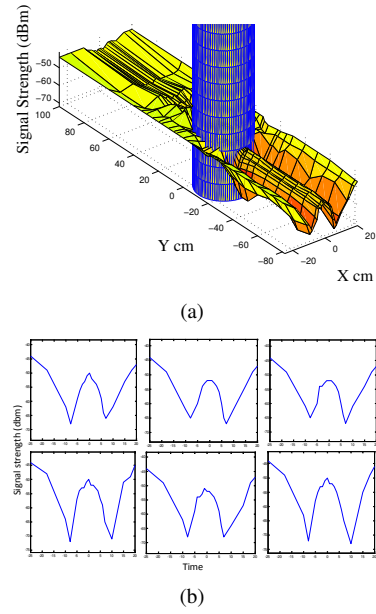


Fig. 4. The RF SS measurements in the 2-D experimental space with the presence of (a) a cylinder obstacle and (b) Different trajectories.

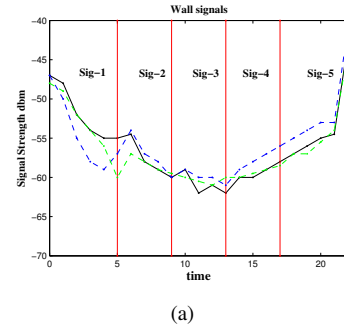


Fig. 5. Segmented wall signals.

$[S_l^{(j)}(1) S_l^{(j)}(2) \dots S_l^{(j)}(N_m)]^T$ , where  $N_m$  represents the number of SS measurements along the  $l$ th trajectory for the  $j$ th obstacle type. Each  $\beta_l^{(j)}$  is segmented into five segments denoted as  $\alpha_{l,u}^{(j)} = [S_l^{(j)}(5(u-1)+1) \dots S_l^{(j)}(5u)]^T$ ,  $u = 1, 2, \dots, 5$  as in Fig. 5. Afterward, each measurement segment  $\alpha_{l,u}^{(j)}$  is transformed into the frequency domain using FFT, and the results of FFT are denoted as  $\Gamma_{l,u}^{(j)} = \text{FFT}(\alpha_{l,u}^{(j)}, N_{FFT})$ , where  $\text{FFT}(\cdot)$  denotes the FFT operation,  $N_{FFT}$  denotes the number of points in the FFT results. The first 10 elements in the FFT result  $\Gamma_{l,u}^{(j)}$  are defined as the feature vector  $\gamma_{l,u}^{(j)} = [\Gamma_{l,u}^{(j)}(1) \Gamma_{l,u}^{(j)}(2) \dots \Gamma_{l,u}^{(j)}(10)]^T$  of the measurement corresponding to the  $l$ th trajectory and  $j$ th obstacle type. Once each segment is transferred into frequency space, the feature vector  $\Gamma_{l,u}^{(j)}$  is clustered using the  $K$ -means clustering algorithm. Then, the HMM uses these binned segments to classify the obstacle shadow based on the probabilistic sequence of segments. In other words, we used spatial distinctions to classify cluster each segment (a phoneme) using  $k$ -means clustering algorithm, and the



Fig. 6. Block diagram of RF environment recognition processing steps.

temporal ordering within the sequence to classify obstacle shadow (a word) using HMM classification method. In our numerical experiments, we tried different training sets to examine their effect on the recognition rate. We found that the recognition rate is affected positively by the size increase of the training sets. Data was randomly split into training and testing sets for the verification of the HMM classifier. We randomly select 60% of the measurement vectors into the training set  $\mathcal{S}_{\text{train}}^c$  which is used for clustering and training, and the rest constitutes the testing set  $\mathcal{S}_{\text{test}}^c$ .

### B. Unsupervised Clustering for Observation Generation

The measurement vectors  $\gamma_{l,u}^{(j)}$  in the training set  $\mathcal{S}_{\text{train}}^c$  are clustered into  $G$  clusters using the  $k$ -means clustering algorithm. We denote the  $G$  clusters as  $\mathcal{D}_1, \mathcal{D}_2, \dots, \mathcal{D}_G$  so that the within-cluster sum of squares (WCSS) is minimized. The  $k$ -means algorithm is summarized in (3) as

$$\arg \min_{\mathcal{D}_1, \dots, \mathcal{D}_G} \sum_{g=1}^G \sum_{\beta_l^{(j)} \in \mathcal{S}_{\text{train}}^c, \gamma_{l,u}^{(j)} \in \mathcal{D}_g} \|\gamma_{l,u}^{(j)} - \mu_g\|^2 \quad (3)$$

where  $\mu_g$  is the centroid of  $\mathcal{D}_g$ , i.e. the mean of points in  $\mathcal{D}_g$ ,  $\|\gamma_{l,u}^{(j)} - \mu_g\|^2$  is the squared Euclidean distance between the vector  $\gamma_{l,u}^{(j)}$  and  $\mu_g$ . After  $\mathcal{D}_g$  and  $\mu_g$  are generated by the  $k$ -means clustering algorithm they are used to assign observation symbols to the feature vectors to generate observation sequences for HMM training and test. First, we denote the symbol set used for representing HMM observations as  $\mathcal{C} = \{C_1, \dots, C_G\}$  with  $C_g$  as the  $g$ th symbol. The symbol  $C_{l,u}^{(j)}$  corresponding to the data segment  $\gamma_{l,u}^{(j)}$  is assigned with the value  $C_g$  if  $\|\gamma_{l,u}^{(j)} - \mu_g\|^2$  has the minimum value among all  $g \in \{1, 2, \dots, G\}$ . In other words,  $C_{l,u}^{(j)}$  is assigned with symbol  $C_g$ , if the closest cluster centroid to the feature vector  $\gamma_{l,u}^{(j)}$  is  $\mu_g$ . We concatenate the  $C_{l,u}^{(j)}$  corresponding to the segments from the  $l$ th trajectory to form the vector  $C_l^{(j)} = [C_{l,1}^{(j)} \dots C_{l,5}^{(j)}]^T$ . The resulting vector  $C_l^{(j)}$  is the *observation sequence* corresponding to measurement vector  $\beta_l^{(j)}$ . Observation sequence  $C_l^{(j)}$  is in the HMM training set  $\mathcal{S}_{\text{train}}^{\text{HMM}}$  if its corresponding measurement vector  $\beta_l^{(j)}$  is in the clustering training set  $\mathcal{S}_{\text{train}}^c$ , otherwise, it is in the HMM test set  $\mathcal{S}_{\text{test}}^{\text{HMM}}$ .

In summary, following the above procedure, an *measurement vector*  $\beta_l^{(j)}$  for the  $l$ th trajectory in the presence of type  $j$  obstacles, is segmented into segments  $\alpha_{l,u}^{(j)}$ ,  $u = 1, 2, 3, 4, 5$ . Consequentially, each  $\alpha_{l,u}^{(j)}$  is transformed into the frequency domain by FFT, and the FFT result is denoted by  $\Gamma_{l,u}^{(j)}$ . The first 10 elements in  $\Gamma_{l,u}^{(j)}$  are selected to form *feature vector*  $\gamma_{l,u}^{(j)}$ . The feature vectors are clustered

using the  $k$ -means clustering algorithm to generate  $G$  clusters,  $\mathcal{D}_1, \dots, \mathcal{D}_G$ , and the corresponding cluster centroids  $\mu_1, \dots, \mu_G$ . Using the cluster parameters, each segment feature vector  $\gamma_{l,u}^{(j)}$  is assigned with a symbol  $C_{l,u}^{(j)} \in \mathcal{C}$ . We concatenate  $C_{l,u}^{(j)}$  to form the *observation sequence*  $C_l^{(j)}$ . At this point, the measurement vector for each trajectory  $\beta_l^{(j)}$  is transformed into observation sequence  $C_l^{(j)}$  and ready for training or testing HMMs.

## IV. NUMERICAL RESULTS ON HMM BASED RECOGNITION

The HMM training set  $\mathcal{S}_{\text{train}}^{\text{HMM}}$  is used to train three HMMs, and each HMM corresponds to one of the three obstacle types. We denote the trained HMMs as  $\lambda_{(p)}$ , with  $j = 1, 2, 3$  corresponding to obstacle type of wall, cage and cylinder, respectively. Given an observation sequence  $C_l^{(j)}$  which are composed of several observation symbols, the conditional probability of  $C_l^{(j)}$  given HMM  $\lambda_{(p)}$ ,  $P(C_l^{(j)} | \lambda_{(p)})$ , is calculated for  $p = 1, 2, 3$  for classification. If the maximum  $P(C_l^{(j)} | \lambda_{(p)})$  is obtained with  $p = \hat{p}$ , we predict that the EMF environment is with obstacle type  $\hat{p}$ . We note that  $C_l^{(j)}$  is an observation sequence with arbitrary length, and thus may only contain the first few available observations. This corresponds to the scenarios where the robots are approaching an obstacle without all the observations being available.

### A. Different cylinder sizes

In this experiment, a total of 535 measurement vectors are used. A subset of 321 measurement vectors are used for training, and the reminder are used for testing. These measurement vectors contain three different cylinder radiuses, which are  $r = 10$  cm,  $r = 15$  cm and  $r = 20$  cm, the height of the cylinders is 30 cm. The confusion matrix of the EMF recognition results are shown in Tables 1, 2 and 3, each row of the confusion matrix represents the predicted class and each column represents the actual class. Table 1 demonstrates the confusion matrix of EMF recognition using the first 2 elements in observation sequences, the classification rate achieved is 84%. Table 2 demonstrates the confusion matrix using the first 3 elements in observation sequences, the success rate is 92% and Table 3 demonstrates the confusion matrix of EMF recognition using 4 elements the classification rate is 100%.

TABLE I  
CONFUSION MATRIX OF EMF RECOGNITION BY 2 OBSERVATIONS.

| Cylinders   | $r = 10$ cm | $r = 15$ cm | $r = 20$ cm |
|-------------|-------------|-------------|-------------|
| $r = 10$ cm | 0.86        | 0.0         | 0.14        |
| $r = 15$ cm | 0.14        | 1           | 0.22        |
| $r = 20$ cm | 0.0         | 0.0         | 0.64        |

TABLE II  
CONFUSION MATRIX OF EMF RECOGNITION BY 3 OBSERVATIONS.

| Cylinders   | $r = 10$ cm | $r = 15$ cm | $r = 20$ cm |
|-------------|-------------|-------------|-------------|
| $r = 10$ cm | 1           | 0.0         | 0.0         |
| $r = 15$ cm | 0.0         | 1           | 0.0         |
| $r = 20$ cm | 0.0         | 0.0         | 1           |

TABLE III  
CONFUSION MATRIX OF EMF RECOGNITION BY 4 OBSERVATIONS.

| Cylinders   | $r = 10$ cm | $r = 15$ cm | $r = 20$ cm |
|-------------|-------------|-------------|-------------|
| $r = 10$ cm | 1           | 0.0         | 0.0         |
| $r = 15$ cm | 0.0         | 1           | 0.0         |
| $r = 20$ cm | 0.0         | 0.0         | 1           |

### B. Different walls, cylinders and cages sizes

In this experiment, a total of a 825 measurement vectors containing the three aforementioned obstacles with different sizes. A subset of 495 measurement vectors are used for training, and a subset of 330 measurement vectors are used for testing. The confusion matrix of the EMF recognition results are shown in Tables 4, 5 and 6, each row of the confusion matrix represents the predicted class and each column represents the actual class. Table 4 demonstrates the confusion matrix of EMF recognition using the first 2 elements in observation sequences the classification rate is 87%. Table 5 demonstrates the confusion matrix using the first 3 elements in observation sequences, the success rate for this experiment is 89% and Table 6 demonstrates the confusion matrix of EMF recognition using 4 elements of the observation sequences the classification rate is 92%. The results show that the HMM classifier can achieve satisfied classification performance when 2 observations are available, and the classification performance improves as more observations become available. Thus, these results demonstrate that the proposed method has sufficient ability in EMF environment recognition for proactive robot planning.

TABLE IV  
CONFUSION MATRIX OF EMF RECOGNITION BY 2 OBSERVATIONS.

| Different obstacles   | Cage<br>$30\text{ cm}^3$ | Wall<br>10 cm | Wall<br>15 cm | Cylinder<br>10 cm | Cylinder<br>15 cm |
|-----------------------|--------------------------|---------------|---------------|-------------------|-------------------|
| Cage $30\text{ cm}^3$ | 1                        | 0.0           | 0.0           | 0.0               | 0.0               |
| Wall $w = 10$ cm      | 0.0                      | 1             | 0.44          | 0.0               | 0.0               |
| Wall $w = 15$ cm      | 0.0                      | 0.0           | 0.56          | 0.0               | 0.0               |
| Cylinder $r = 10$ cm  | 0.0                      | 0.0           | 0.0           | 0.80              | 0.0               |
| Cylinder $r = 15$ cm  | 0.0                      | 0.0           | 0.0           | 0.20              | 1                 |

TABLE V  
CONFUSION MATRIX OF EMF RECOGNITION BY 3 OBSERVATIONS.

| Different obstacles   | Cage<br>$30\text{ cm}^3$ | Wall<br>10 cm | Wall<br>15 cm | Cylinder<br>10 cm | Cylinder<br>15 cm |
|-----------------------|--------------------------|---------------|---------------|-------------------|-------------------|
| Cage $30\text{ cm}^3$ | 1                        | 0.0           | 0.0           | 0.0               | 0.0               |
| Wall $w = 10$ cm      | 0.0                      | 0.34          | 0.0           | 0.0               | 0.0               |
| Wall $w = 15$ cm      | 0.0                      | 0.66          | 1             | 0.0               | 0.0               |
| Wall $r = 10$ cm      | 0.0                      | 0.0           | 0.0           | 0.80              | 0.0               |
| Cylinder $r = 15$ cm  | 0.0                      | 0.0           | 0.0           | 0.20              | 1                 |

TABLE VI  
CONFUSION MATRIX OF EMF RECOGNITION BY 4 OBSERVATIONS.

| Different obstacles   | Cage<br>$30\text{ cm}^3$ | Wall<br>10 cm | Wall<br>15 cm | Cylinder<br>10 cm | Cylinder<br>15 cm |
|-----------------------|--------------------------|---------------|---------------|-------------------|-------------------|
| Cage $30\text{ cm}^3$ | 1                        | 0.0           | 0.0           | 0.0               | 0.0               |
| Wall $w = 10$ cm      | 0.0                      | 1             | 0.40          | 0.0               | 0.0               |
| Wall $w = 15$ cm      | 0.0                      | 0.0           | 0.60          | 0.0               | 0.0               |
| Cylinder $w = 10$ cm  | 0.0                      | 0.0           | 0.0           | 1                 | 0.0               |
| Cylinder $w = 10$ cm  | 0.0                      | 0.0           | 0.0           | 0.0               | 1                 |

## V. MOTION CONTROL ALGORITHM FOR CONNECTIVITY MAINTENANCE

In the application scenario, when a moving robot starts to lose communication connectivity with the team, its motion

control mechanism will guide the robots towards favorable positions in the field for maintaining the connectivity or fixing the failing link. The motion control algorithm needs to utilize the knowledge learned from EMF recognition through HMM results. Once the robot recognizes the obstacle shadow or obstacle type, the motion control algorithm will decide whether the robots continue their trajectories or move the robots back to a position in the field where the robots can gain a strong signal strength. The motion control algorithm takes the first decision, it drives the robots to move across the obstacle shadow towards a favorable position to maintain their connectivity based on the HMM results. If the motion control algorithm chooses the second decision, the robots start computing the gradient to find the trend of the strong SS and then maintain their connectivity. We use the gradient based motion control algorithm, by which the multi-dimension gradient of the SS measurements is extracted for controlling robot movement around the obstacle. In other words, the motion control algorithm has the decision to continue the movement through the obstacle shadow or to move back to a position in the field that has a strong enough SS, and computes the gradient to define the direction of robots movement to maintain their connectivity, depending on the HMM results that estimate the type and the approximate size of the obstacle. The flowchart in Fig. 7 summarizes the main steps of the motion control algorithm.

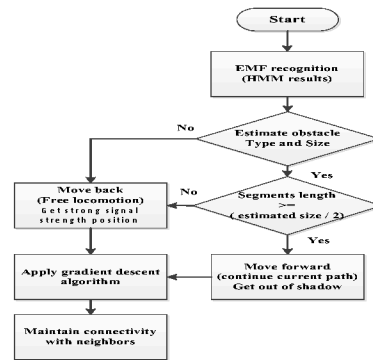


Fig. 7. Flowchart diagram of the motion control algorithm

### A. Gradient based Motion Control

In the SS gradient experiments, we start with a simple scenario where two mobile robots transmit and receive RF signals, respectively. The sensor measures SS at the receiver location. The two robots are separated by distance  $d$  along the  $x$ -direction as shown in Fig. 1 (b). The signal strength  $S_l^{(j)}(k)$  at time  $k$  for the  $l$ th trajectory in the presence of obstacle type  $j$  can be calculated according to (2) defined in Section 2.1.

As the robots move in the EMF environment with LOS between each other, the signal strength  $S_l^{(j)}(k)$  remains stable. However, if a conductive obstacle appears in the experiment field, the  $S_l^{(j)}(k)$  is subject to change as the robots move around the obstacle. In this scenario, the SS measurements,  $S_l^{(j)}(k)$ , resulted from the two moving robots are to be measured and recorded for each  $(x_k^{(i)}, y_k^{(i)})$ ,  $i = 1, 2$

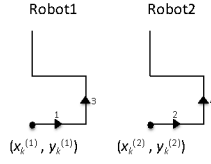


Fig. 8. Step wise trajectory of two robots as transmitter and receiver.

at time  $k$ . We then extract the 4-D gradient vector of the SS corresponding to known trajectories. The gradient vector of the SS at time  $k$  for the  $l$ th trajectory is defined as

$$\nabla S_l^{(j)}(k) = \left[ \frac{\partial S_l^{(j)}(k)}{\partial x_k^{(1)}} \quad \frac{\partial S_l^{(j)}(k)}{\partial y_k^{(1)}} \quad \frac{\partial S_l^{(j)}(k)}{\partial x_k^{(2)}} \quad \frac{\partial S_l^{(j)}(k)}{\partial y_k^{(2)}} \right]^T \quad (4)$$

In typical scenarios, robots would move in parallel straight-lines to reach their goal. However, this leads to undefined gradient estimates because the sampling locations can not be co-linear. Therefore, rather than traveling in parallel straight-lines trajectories, the robots introduces some dither or oscillations to their paths as shown in Fig. 8. This makes the gradient estimation more robust at the cost of distance. We calculate the SS gradient using the trajectories as shown in Fig. 8 where we assume robot 1 and robot 2 are located at positions  $(x_k^{(1)}, y_k^{(1)})$  and  $(x_k^{(2)}, y_k^{(2)})$  at time  $k$ , respectively. If only one robot moves at a time and the other stays still, the gradient can be calculated using the following method. Fig. 8 shows the step wise trajectories for the two mobile robots for calculating the gradient vector. During time  $k$  and  $k+1$ , robot 1 moves along trajectory segment 1, so  $x_{k+1}^{(1)} = x_k^{(1)} + \Delta x$ ,  $y_{k+1}^{(1)} = y_k^{(1)}$ ,  $x_{k+1}^{(2)} = x_k^{(2)}$ ,  $y_{k+1}^{(2)} = y_k^{(2)}$ , and the gradient element  $\frac{\partial S_l^{(j)}(k)}{\partial x_k^{(1)}}$  is calculated as

$$\frac{\partial S_l^{(j)}(k)}{\partial x_k^{(1)}} \approx \frac{\Delta S_l^{(j)}(k)}{\Delta x_k^{(1)}} = \frac{S_l^{(j)}(k+1) - S_l^{(j)}(k)}{\Delta x} \quad (5)$$

During time  $k+1$  and  $k+2$ , robot 2 moves along trajectory segment 2, so  $x_{k+2}^{(1)} = x_{k+1}^{(1)}$ ,  $y_{k+2}^{(1)} = y_{k+1}^{(1)}$ ,  $x_{k+2}^{(2)} = x_{k+1}^{(2)} + \Delta x$ ,  $y_{k+2}^{(2)} = y_{k+1}^{(2)}$ , and the gradient element is  $\frac{\partial S_l^{(j)}(k)}{\partial x_k^{(2)}}$  calculated as

$$\frac{\partial S_l^{(j)}(k)}{\partial x_k^{(2)}} \approx \frac{\Delta S_l^{(j)}(k+1)}{\Delta x_{k+1}^{(2)}} = \frac{S_l^{(j)}(k+2) - S_l^{(j)}(k+1)}{\Delta x} \quad (6)$$

During time  $k+2$  and  $k+3$ , robot 1 moves along trajectory segment 3, so  $x_{k+3}^{(1)} = x_{k+2}^{(1)}$ ,  $y_{k+3}^{(1)} = y_{k+2}^{(1)} + \Delta y$ ,  $x_{k+3}^{(2)} = x_{k+2}^{(2)}$ ,  $y_{k+3}^{(2)} = y_{k+2}^{(2)}$ , and the gradient element  $\frac{\partial S_l^{(j)}(k)}{\partial y_k^{(1)}}$  is calculated as

$$\frac{\partial S_l^{(j)}(k)}{\partial y_k^{(1)}} \approx \frac{\Delta S_l^{(j)}(k+2)}{\Delta y_{k+2}^{(1)}} = \frac{S_l^{(j)}(k+3) - S_l^{(j)}(k+2)}{\Delta y} \quad (7)$$

During time  $k+3$  and  $k+4$ , robot 2 moves along trajectory segment 4, so  $x_{k+4}^{(1)} = x_{k+3}^{(1)}$ ,  $y_{k+4}^{(1)} = y_{k+3}^{(1)}$ ,  $x_{k+4}^{(2)} = x_{k+3}^{(2)}$ ,  $y_{k+4}^{(2)} = y_{k+3}^{(2)} + \Delta y$ , and the gradient element  $\frac{\partial S_l^{(j)}(k)}{\partial y_k^{(2)}}$  is calculated as

$$\frac{\partial S_l^{(j)}(k)}{\partial y_k^{(2)}} \approx \frac{\Delta S_l^{(j)}(k+3)}{\Delta y_{k+3}^{(2)}} = \frac{S_l^{(j)}(k+4) - S_l^{(j)}(k+3)}{\Delta y} \quad (8)$$

As we can see in Fig. 9 (a), when the two robots have the LOS between each other, their reception SS is strong, which is indicated by yellow boxes, and their gradient directions point towards each other, which is indicated by arrows. However, when one of the robots is trapped inside the cage, the gradient amplitudes become small, which is indicated by green boxes. The movements of the robot which is outside of the cage do not result in a noticeable increase of the SS. However, as we can see in Fig. 9(a), small movement of the trapped robot result in a significant increase of the SS once it leaves the cage. In Fig. 9(b), the robot moves extremely close to the cage in a step wise trajectory while the other robot is stands still on the left side of the cage. The gradient points along the direction of the other robot in the presence of LOS and it is subject to scatter when the obstacle blocks the two robots.

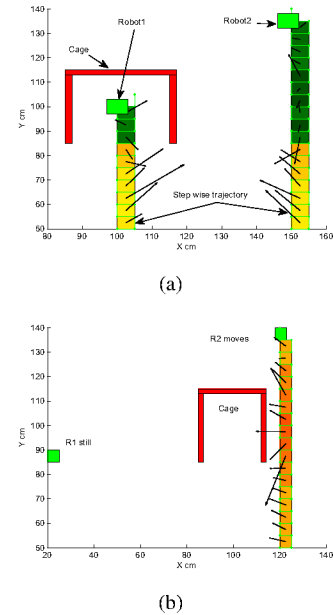


Fig. 9. (a) Two robots move in the experiment field, with one trapped in the cage, and the (b)The left robot stays still and right robot moves in stepwise trajectory.

Fig. 10(a) shows the SS gradient direction and SS magnitude for the scenario when one robot is close to one corner of the cage while the other one moves in a step wise around the cage. The gradient points toward the other robot when there is a LOS, and it subject to scatter as the robots separated by an obstacle. The observation from Fig. 9(b) and Fig. 10 (a) shows that gradient directions can lead the robots to the favorable positions to maintain their connectivity. Fig. 10 (b) shows a scenario where two robots move in parallel one at a time along different trajectories around the cage. The robot at the left side moves two segments in a step wise trajectory, one segment in  $x$ -direction and the other one in  $y$ -direction while the other robot stands till. Then, the stands

still robot moves one segment in  $y$ -direction along a straight line trajectory and this process repeated along each trajectory in the experiment field. In this experiment, the gradient is calculated for the right robot according to (5) and (7). The gradient directions and magnitudes of the SS are shown at each position. This confirms that the gradients are useful in finding favorable locations to maintain RF links between robots.

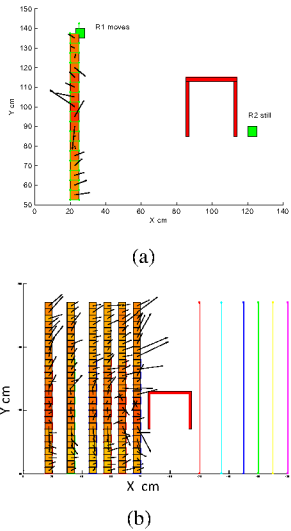
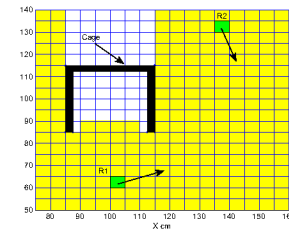


Fig. 10. (a) The right robot stays still and the right robot moves in stepwise trajectory, and (b) Two robots move at the two sides of the cage.

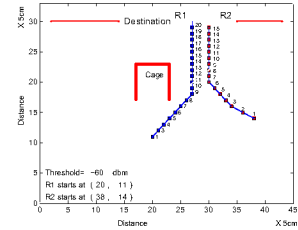
### B. The Gradient Algorithm Results

The idea of the motion control algorithm is to divide the experiment field of the robots into grids as explained in Section 2.1. shown in Fig. 11(a), two robots move in the area defined by yellow grids, measure the SS and calculate the gradient for any two points in the field for motion control. A database is established which contains the robots' positions, SS measurements, and gradient calculation results at each time  $k$ . The flowchart of the gradient algorithm is shown in Fig. 12. Fig. 11(b) shows two robots trajectories where robot 1 starts at  $x_0^{(1)} = 20, y_0^{(1)} = 11$  and robot 2 starts at  $x_0^{(2)} = 38, y_0^{(2)} = 14$  at time  $k = 0$  in the experiment field. The gradient algorithm drives the robots to avoid the obstacle shadow and maintain their connectivity. Fig. 13 (a) shows two trajectories where robot 1 starts at  $(x_0^{(1)} = 17, y_0^{(1)} = 15)$  at the entrance of the cage obstacle and robot 2 starts at  $(x_0^{(2)} = 38, y_0^{(2)} = 15)$  on the right side of the obstacle at time  $k = 0$ . Both trajectories show that the gradient algorithm can guide the robots to approach each other to evade the obstacle effects and maintain the robots' connectivity.

The scenario in Fig. 13(b) shows two robots trajectories where robot 1 starts at  $x_0^{(1)} = 22, y_0^{(1)} = 17$  and robot 2 starts at  $x_0^{(2)} = 40, y_0^{(2)} = 23$  at time  $k = 0$ . This experiment illustrates how the algorithm performs when robot 1 faces the obstacle while robot 2 moves far right most of an obstacle.



(a)



(b)

Fig. 11. (a) Configuration space of Two robots, and (b) Robots start at  $x_0^{(1)} = 20, y_0^{(1)} = 11$  and  $x_0^{(2)} = 38, y_0^{(2)} = 14$  at time  $k=0$ .

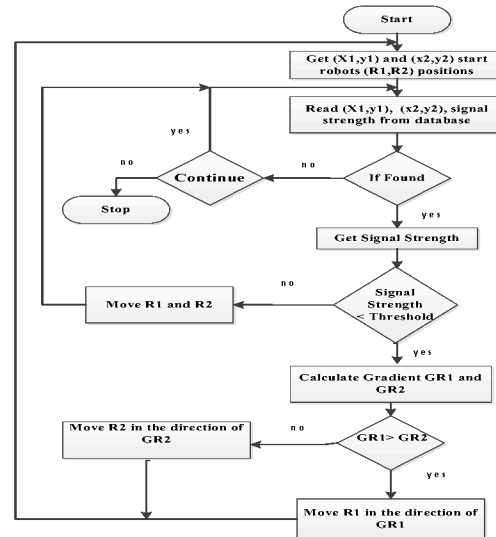
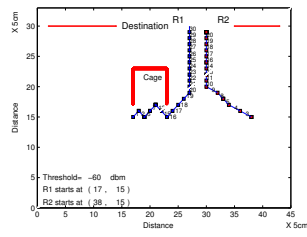


Fig. 12. Gradient Algorithm flowchart.

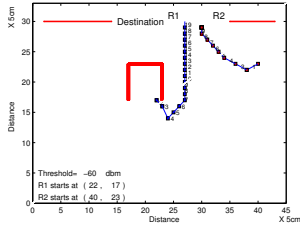
It is clear that the gradient algorithm has the ability to drive the robots safely and maintain their connectivity.

### C. The Motion Control Algorithm Results

The HMM results through EMF recognition demonstrates detection of an obstacle on the robot trajectory and confirms the obstacle type and approximate size within specific distance along the robot path. The motion control algorithm uses the HMM results to drive robots to continue moving forward through the current trajectories if the segments length traveled by the robots are greater than or equal one half of the estimated obstacle size as shown in the scenario of Fig. 14 (a). Otherwise, the robots stop movement and move back to a position where it can gain strong SS. Then, the

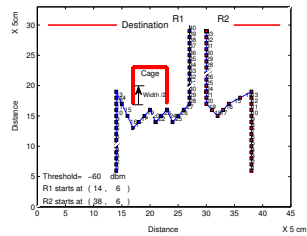


(a)

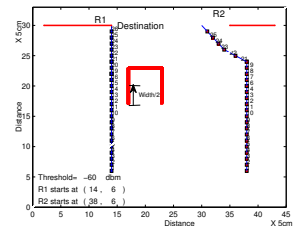


(b)

Fig. 13. (a) Robots start at  $x_0(1) = 17, y_0(1) = 15$  and  $x_0(2) = 38, y_0(2) = 15$  at time  $k=0$ , and (b) Robots start at  $x_0(1) = 22, y_0(1) = 17$  and  $x_0(2) = 40, y_0(2) = 23$  at time  $k=0$ .



(a)



(b)

Fig. 14. Control Robots movement using (a) two observations (b) three observations)

robots run the gradient algorithm to define the direction of the strongest SS. Afterwards, the robots move in the direction of the gradient and attempt to regain communication as shown in the scenario of Fig. 14 (b). Fig. 7 summarizes the main steps of the motion control algorithm.

## VI. CONCLUSION

In this paper, an EMF environment recognition approach and a gradient based robot motion control method were presented. Extensive numerical simulations were conducted to evaluate the feasibility and performance of the proposed EMF environment recognition and gradient based motion

control. The proposed methods have presented preliminary studies and promising solutions to joint physical message routing and logical link maintenance in robots network. We expect that the proposed methods can be a competitive alternative to broken link replacement and maintain robot connectivity in robotic networks. We can achieve that through controlling the movement of mobile robots in the field.

## ACKNOWLEDGEMENTS

This work was sponsored in part by the NSF Safety, Security and Rescue Research Center and by the NSF under grants No.719306 and 0923518. Opinions expressed are those of the authors and are not necessarily endorsed by the NSF.

## REFERENCES

- [1] J. Sweeney, T.J. Brunette, Y. Yang, and R. Grupen, "Coordinated teams of reactive mobile platforms," in *IEEE International Conference on Robotics and Automation (ICRA)*, 2002, vol. 1, pp. 299–304.
- [2] N. Michael, M.M. Zavlanos, V. Kumar, and G.J. Pappas, "Maintaining connectivity in mobile robot networks," in *International Symposium on Experimental Robotics*, Athena, Greece, July 2009.
- [3] M. Lindhe, H. Johansson, and A. Bicchi, "An experimental study of exploiting multipath fading for robot communications," in *Proceeding of Robotics: Science and Systems*, Atlanta, CA, June 2007.
- [4] J. Bae and R.M. Voyles, "Wireless video sensor network from a team of urban search and rescue robot," in *International Conference on Wireless Networks*, 2006.
- [5] J.N. Twigg, J.R. Fink, P.L. Yu, and B.M. Sadler, "Rss gradient-assisted frontier exploration and radio source localization," in *IEEE International Conference on Robotics and Automation (ICRA)*, May 2012, pp. 889–895.
- [6] Yi Sun, Jizhong Xiao, Xiaohai Li, and F. Cabrera-Mora, "Adaptive source localization by a mobile robot using signal power gradient in sensor networks," in *IEEE Global Telecommunications Conference*, Dec 2008, pp. 1–5.
- [7] J. Fink, V. Kumar, N. Michael, and A. Kushleyev, "Experimental characterization of radio signal propagation in indoor environments with application to estimation and control," in *IEEE International Conference on Intelligent Robots and Systems*, 2009.
- [8] J. Fink and V. Kumar, "Online methods for radio signal mapping with mobile robots," in *IEEE International Conference on Robotics and Automation (ICRA)*, 2010.
- [9] M.A. Hsieh, A. Cowley, V. Kumar, and C. J. Taylor, "Maintaining network connectivity and performance in robot teams," *Journal of Field Robotics*, vol. 25, no. 1, pp. 111–131, Jan 2008.
- [10] F. Zeiger, N. Kraemer, and K. Schilling, "Commanding mobile robots via wireless ad-hoc networks - a comparison of four ad-hoc routing protocol implementations," in *IEEE International Conference on Robotics and Automation (ICRA)*, 2008.
- [11] "CST microwave studio," <http://www.cst.com/MWS/Overview.aspx>.
- [12] D. Jurafsky and J. H. Martin., "Speech and language processing," in *Prentice Hall, Inc.*, 2000.
- [13] L.R. Rabiner, "A tutorial on hidden Markov models and selected applications in speech recognition," Feb 1989, vol. 77, pp. 257–286.